International Journal of Biological Macromolecules

Research article

Crystal structure of a novel type of ornithine δ-aminotransferase from the hyperthermophilic archaeon *Pyrococcus horikoshii*

Ryushi Kawakami [a], Tatsuya Ohshida [b], Junji Hayashi [a], Kazunari Yoneda [c], Toshio Furumoto [b], Toshihisa Ohshima [d], and Haruhiko Sakuraba [b, *]

[a]Division of Bioscience and Bioindustry, Graduate school of Technology, Industrial and Social Sciences, Tokushima University, 2-1, Minamijosanjima-cho, Tokushima, Tokushima 770-8513, Tokushima, Japan

[b]Department of Applied Biological Science, Faculty of Agriculture, Kagawa University, 2393 Ikenobe, Miki-cho, Kita-gun, Kagawa, 761-0795, Japan

[c]Department of Bioscience, School of Agriculture, Tokai University, 9-1-1 Toroku, Higashi-ku, Kumamoto-shi, Kumamoto, 862-8652, Japan

[d]Department of Biomedical Engineering, Faculty of Engineering, Osaka Institute of Technology, 5-16-1 Ohmiya, Asahi-ku, Osaka, 535-8585, Japan.

* Corresponding author

E-mail address: sakuraba.haruhiko@kagawa-u.ac.jp (H. Sakuraba)

Highlights

- The crystal structures of a novel archaeal type of ornithine δ-aminotransferase were determined.
- The structure of the enzyme in complex with its natural substrate revealed that the substrate recognition residues are notably different from those of human ornithine δ-aminotransferase.
- The structure of the enzyme in complex with its natural external aldimine provides the first structural evidence for the “Glu switch” mechanism in the dual substrate specificity of ornithine δ-aminotransferase.

Abstract

Ornithine δ-aminotransferase (Orn-AT) activity was detected for the enzyme annotated as a γ-aminobutyrate aminotransferase encoded by PH1423 gene from *Pyrococcus horikoshii* OT-3. Crystal structures of this novel archaeal ω-aminotransferase were determined for the enzyme in complex with pyridoxal 5’-phosphate (PLP), in

complex with PLP and L-ornithine (L-Orn), and in complex with *N*-(5'-phosphopyridoxyl)-L-glutamate (PLP-L-Glu). Although the sequence identity was relatively low (28%), the main-chain coordinates of *P. horikoshii* Orn-AT monomer showed notable similarity to those of human Orn-AT. However, the residues recognizing the α-amino group of L-Orn differ between the two enzymes. In human Orn-AT, Tyr55 and Tyr85 recognize the α-amino group, whereas the side chains of Thr92* and Asp93*, which arise from a loop in the neighboring subunit, form hydrogen bonds with the α-amino group of the substrate in *P. horikoshii* enzyme. Site-directed mutagenesis suggested that Asp93* plays critical roles in maintaining high affinity for the substrate. This study provides new insight into the substrate binding of a novel type of Orn-AT. Moreover, the structure of the enzyme with the reaction-intermediate analog PLP-L-Glu bound provides the first structural evidence for the "Glu switch" mechanism in the dual substrate specificity of Orn-AT.

Keywords:

ornithine aminotransferase, archaea, crystal structure

1. Introduction

ω-Aminotransferases catalyze the transfer of an amino group which is distal to the α-carboxyl group [1] and comprise the majority of the class III aminotransferases, which belong to the fold type I pyridoxal 5'-phosphate (PLP)-dependent enzyme [2]. ω-Aminotransferases play a crucial role in the metabolism of physiologically important substances, e.g. γ-aminobutyrate (GABA) and L-ornithine (L-Orn). GABA is the major inhibitory neurotransmitter in the mammalian brain. Degradation of GABA is achieved through the reaction of GABA aminotransferase (GABA-AT), in which GABA is converted into succinic semialdehyde using 2-oxoglutarate as co-substrate. Thus, GABA-AT is an established target for neuroactive drugs [3]. On the other hand, L-Orn acts in the urea cycle as a mediator for the removal of ammonia and plays a pivotal role in cell detoxification [4]. Ornithine δ-aminotransferase (Orn-AT, EC 2.6.1.13) catalyzes the first-step reaction of the major catabolic pathway of L-Orn. In humans, Orn-AT dysfunction causes hyperornithinemia and gyrate atrophy [5]. The enzyme catalyzes the ω (δ)-amino group transfer of L-Orn to 2-oxoglutarate, yielding L-glutamate (L-Glu) and L-glutamate 5-semialdehyde, which spontaneously cyclizes to form L-1-pyrroline-5-carboxylate (P5C) [6].

In the case of GABA-AT, the amino group transferred is the only amino group (ω-amino group) in GABA molecule, whereas in the case of Orn-AT, ω-amino group among

the two different α and ω-amino groups in L-Orn molecule is specifically transferred to 2-oxoglutarate. In general, PLP-dependent transamination reactions proceed in ping-pong mechanisms via PMP (pyridoxamine phosphate) intermediate form of enzyme and consist of two half reactions. In the case of Orn-AT (PLP-form), L-Orn is converted to L-glutamate 5-semialdehyde and the PMP-form intermediate is produced in the first half reaction. In the second half-reaction, 2-oxoglutarate binds to the intermediate and after transamination, L-Glu and PLP-form enzyme are produced as the final product (Fig. 1). This means that the enzyme can selectively recognize the ω-amino group of L-Orn and the α-amino group of L-glutamate for the two half reactions [7]. However, the "Glu switch" mechanism in the dual substrate specificity of Orn-AT remains to be fully elucidated.

Orn-AT and GABA-AT occur widely in both Bacteria and Eukarya. Recently, an Orn-AT has been detected in the hyperthermophilic archaeon *Thermococcus kodakarensis* and reported to be required for its growth in the absence of exogenous proline [8]. That enzyme is the only archaeal Orn-AT so far reported, and genetic analysis confirmed its physiological function as the enzyme involved in the biosynthesis of L-proline. Interestingly, the amino acid sequence of the *T. kodakarensis* Orn-AT (TK2101) is not similar to the previously reported sequences of bacterial and eukaryotic Orn-ATs. The enzyme was originally annotated as GABA-AT in the genome database, and phylogenetic

analysis revealed that the clade containing *T. kodakarensis* Orn-AT is clearly distinct from that of previously characterized Orn-ATs [8].

We have been focusing on GABA-AT homologs from *Pyrococcus* and *Thermococcus* strains. The genome database (KEGG: Kyoto Encyclopedia of Genes and Genomes) for *P. horikoshii* includes four GABA-AT genes, PH0138, PH0782, PH1501, and PH1423, whose products share more than 45% amino acid sequence identity with one another. Among these GABA-AT homologues, the PH1423 gene product shares nearly 60% sequence identity with *T. kodakarensis* Orn-AT and exhibits a high level of Orn-AT activity [9]. Like *T. kodakarensis* Orn-AT, that enzyme utilized L-Orn and 2-oxoglutarate as the most preferable substrates as the amino donor and acceptor, respectively (this study). A structural analysis of the PH1423 gene product may shed light on the substrate-recognition mechanism of a novel group of archaeal Orn-ATs, which are phylogenetically distant from conventional Orn-ATs.

Here, we report the basic enzymatic properties of *P. horikoshii* Orn-AT (PH1423 gene product) and the structures of the enzyme binding its natural substrate, L-Orn, and the reaction-intermediate analogue *N*-(5'-phosphopyridoxyl)-L-glutamate (PLP-L-Glu) in addition to the substrate-free enzyme structure. We then compared the architecture of the active site with that of human Orn-AT. This is the first description of the structure of a

novel type of Orn-AT that is widely distributed in *Pyrococcus* and *Thermococcus* strains.

2. Experimental procedures

2.1. Cloning, expression, and purification

The expression plasmid (pET15b/PH1423) was constructed as described previously [10], except that pET11a was replaced with pET15b. *E. coli* BL21 (DE3) CodonPlus RIPL (Stratagene, Tokyo, Japan) cells harboring pET15b/PH1423 were cultivated [10], and gene expression was induced by incubating the cells for 3 h with isopropyl-β-D-thiogalactopyranoside. The cells were then collected by centrifugation, suspended in 10 mM Tris/HCl (pH 8.0), treated with lysozyme, and disrupted by sonication. After centrifugation, the resultant crude extract was heated for 30 min at 90°C and centrifuged to remove the precipitate. The resultant enzyme solution supplemented with 0.5 M NaCl and 0.01 M imidazole was applied to a Co^{2+}-chelating Sepharose (Cytiva, Tokyo) column equilibrated with 10 mM Tris/HCl (pH 8.0) buffer containing 0.5 M NaCl and 0.01 M imidazole. The column was then washed with the same buffer, and the enzyme was eluted with 0.5 M imidazole in the buffer. The column chromatography was performed using peristaltic pump. After dialysis against 10 mM Tris/HCl (pH 8.0), the enzyme was used for characterization and crystallization.

To obtain the enzyme bound with the reaction-intermediate analogue PLP-L-Glu, we first prepared PLP-free apo-enzyme. The crude extract was dialyzed against 10 mM Tris/HCl (pH 8.0) and then applied to Co^{2+}-chelating Sepharose without heat treatment. The column was then washed with the buffer supplemented with 4 M guanidine HCl, incubated for 30 min at room temperature, and further washed with the buffer without guanidine HCl. The refolded enzyme was eluted with the buffer containing 0.5 M imidazole. The purified enzyme was then concentrated up to about 5 mg/ml, mixed with 1 mM PLP-L-Glu, and heated for 20 min at 80°C. This heat treatment step is required for correct reconstitution of the apo-enzyme (see below). After cooling, the buffer in the enzyme solution was changed to 10 mM Tris/HCl (pH 8.0) and concentrated by ultrafiltration using an Amicon Ultra 30k MWCO (Millipore, Tokyo) for crystallization trials.

Protein concentrations were determined with a protein assay kit (Bio-Rad, Tokyo) with bovine serum albumin serving as the standard.

2.2. Molecular mass determination

The molecular mass of the enzyme was analyzed by gel filtration chromatography using a UP SW3000 column (Tosoh, Tokyo). Buffer composed of 50 mM Tris/HCl (pH

7.5) and 0.2 M NaCl was used as the mobile phase at flow rate of 0.35 ml/min. Thyroglobulin (669 kDa), ferritin (440 kDa), aldolase (158 kDa), conalbumin (75 kDa), ovalbumin (44 kDa), carbonic anhydrase (29 kDa), ribonuclease (13.7 kDa), and aprotinin (6.5 kDa) were used as the molecular mass standards.

2.3. Site-directed mutagenesis

To construct mutant (T92V and D93L) plasmids, non-PCRs using PrimestarMax DNA polymerase (Takara, Tokyo) were carried out using TOPO/PH1423 plasmid [10] as the template with the primer sets listed in Supplementary Table 1. The genes in the resultant plasmids were sequenced and subcloned into pET15b. The mutant enzymes were purified using the same method used for the wild-type enzyme.

2.4. Enzyme assays

Orn-AT activity was assayed by measuring the amount of P5C produced from L-Orn by the enzyme reaction. In this case, *o*-aminobenzaldehyde was used for the derivatization of P5C. The reaction mixture (0.2 ml) was composed of 100 mM HEPES/NaOH (pH 7.5), 10 mM L-Orn, 10 mM 2-oxoglutarate, 5 mM *o*-aminobenzaldehyde, 0.04 mM PLP, and 1 μg of enzyme, and the reaction was run for 10 min at 60°C. After cooling on ice for 10

min, the amount of P5C was determined at 440 nm (adsorption coefficient: 1.9 $cm^{-1}mM^{-1}$) [11]. When L-lysine (L-Lys) was used as the substrate, the 2-aminoadipate 6-semialdehyde produced spontaneously cyclized to form L-1-piperideine-6-carboxylate. The adsorption coefficient (2.8 $cm^{-1}mM^{-1}$ at 465 nm) for the L-1-piperideine-6-carboxylate derivative with *o*-aminobenzaldehyde was used to assess activity [12].

2.5. Enzymatic characterization

To determine the amino acceptor specificity of the enzyme, L-Orn was used as the amino donor. L-Glu, L-Ala, and L-Asp produced from 2-oxoglutarate, pyruvate, and oxaloacetate, respectively, were quantitatively determined using reverse phase on an ultra-performance liquid chromatography system (Jasco, Tokyo) [10]. To determine the amino donor specificity, β-alanine, GABA, 5-aminovalerate, 6-aminohexanoate, 2,3-diaminopropionate, 2,4-diaminobutylate, DL-Orn, and DL-Lys were used as amino donors, and 2-oxoglutarate was used as the amino acceptor. After the reaction mixture (0.1 ml) composed of 100 mM HEPES/NaOH (pH 7.5), 10 mM amino donor, 10 mM amino acceptor, 0.04 mM PLP, and 10 μg of enzyme was incubated for 10 min at 60°C, the reaction was stopped by addition of trichloroacetic acid, and NaOH was added to the mixture for neutralization. The amino acid produced by the reaction was derivatized with

o-phthalaldehyde and *N*-butyloxycarbonyl-L-cysteine. The derivatized amino acids were analyzed using an X-press Pak V-C18 column (Jasco).

To assess its apparent thermal stability, the enzyme (0.1 mg/ml) was incubated for 2-24 h at 80°C, after which residual activity was determined by spectrophotometric assay. To assess its pH stability, the enzyme (0.1 mg/ml) was incubated for 0.5 h at 80°C in selected buffers (0.1 M) (citrate/sodium citrate, pH 3.0 and 4.0; acetate/sodium acetate, pH 5.0 and 6.0, HEPES/NaOH, pH 7.0 and 8.0, CHES/NaOH, pH 9.0 and 10.0; and K_2HPO_4/NaOH, pH 11.0 and 12.0), after which the residual activity was then determined. In addition, the thermal and pH dependencies of the enzyme activity were determined with spectrophotometric assays using various temperatures (50-90°C) and buffers (acetate/sodium acetate; pH 5.0-6.5, MES/NaOH; pH 5.0-7.0, KH_2PO_4/K_2HPO_4; pH 6.0-8.0, HEPES/NaOH; pH 6.5-8.5, and Tris/HCl; pH 7.0-9.0).

Kinetic analysis was also performed using spectrophotometric assay. The enzyme activity was determined at several concentrations of L-Orn, D-Orn, L-Lys or D-Lys with a constant concentration of 2-oxoglutarate and at several concentrations of 2-oxoglutarate with a constant concentration of L-Orn, D-Orn, L-Lys or D-Lys.

2.6. Synthesis of PLP-L-Glu

We prepared PLP-L-Glu using a modification of the method previously reported for the synthesis of *N*-(5'-phosphopyridoxyl)-L-isoleucine [13]. A reaction mixture containing 2 mmol of L-Glu and 0.4 mmol of PLP (pH was adjusted to 9.3 with NaOH) was filled to a volume of 20 ml with H_2O. This solution was stirred for 60 min at 25°C, after which 2 ml of 0.1 M NaOH containing 5.2 mmol of $NaBH_4$ was added to reduce the Schiff base formed between PLP and L-Glu. After the solution was decolorized, 22 ml of 0.2 M formic acid was added. The mixture was then loaded onto a Dowex 1×8 (200-400 mesh) (Fujifilm, Osaka, Japan) column (1.4 × 7 cm) previously equilibrated with 0.1 M formic acid, and the column was washed with 0.1 M formic acid (30 ml). PLP-L-Glu was then eluted with a linear gradient from 0.1 to 1.0 M formic acid (30 ml + 30 ml). Fractions containing PLP-L-Glu were confirmed using thin-layer chromatography with a PE-SIL-G/UV TLC plate (Whatman, United Kingdom). 1-Butanol saturated with 1 M HCl was used as the mobile phase. The spots of PLP-L-Glu were localized with a UV illuminator. The pooled fractions were lyophilized and stored at -20°C until use. The ^{1}H-NMR analysis of the product was performed using JNM-ECZ500R FT NMR spectrometer (JEOL, Tokyo, Japan) [500 MHz, D_2O (99.9 atom% D)]. The spectrum showed peaks at 8.46 ppm (1H, s), 4.85 ppm (2H, m), 4.40 ppm (1H, d, J = 14.2 Hz), 4.35 ppm (1H, d, J = 14.2 Hz), 3.75 ppm (1H, t, J = 5.7 Hz), 2.48 ppm (3H, s), 2.35 ppm (2H, m), 2.16 ppm (2H, m).

2.7. Crystallization and data collection

The purified enzymes (substrate-free enzyme and PLP-L-Glu-bound enzyme) were concentrated to about 12 mg/ml by ultrafiltration. The initial screening for crystallization of the enzyme was carried out using the sitting drop vapor diffusion method with Crystal Screen and Crystal Screen 2 (Hampton Research, Aliso Veijo, CA) and Wizard I and II (Rigaku Reagent, Bainbridge Island, WA). Crystals were grown in drops composed of 2 µl of enzyme solution and 2 µl of crystallization buffer at 25°C. An Additive Screening kit (Hampton Research) was used for optimization of the conditions. The substrate-free enzyme was crystallized in the presence of 0.1 M cacodylate (pH 6.0), 11% PEG3000 and 0.2 M $MgCl_2$, and 1 µl of 30% glycerol was added to the drop solution. Crystals of the enzyme with L-Orn bound were prepared by soaking the crystals for 30 h in reservoir solution containing 10 mM L-Orn. Crystals of the enzyme with PLP-L-Glu bound were prepared using the micro-seeding method with a Seed Bead kit (Hampton Research). Crystals of substrate-free enzyme were crushed and added to a drop prepared using PLP-L-Glu-bound enzyme, which was then equilibrated for 18-24 h with reservoir solution. The same procedure was repeated twice, and the resultant crystals were used for diffraction analysis.

Data were collected using a Dectris Pilatus3 S2M detector system on the AR-NW12A beamline at the Photon Factory, Tsukuba, Japan. Measurements were carried out on a crystal cooled to 100 K in a stream of nitrogen gas. Cryoprotection was performed with mother liquor containing 30% (v/v) ethylene glycol. The data were processed using HKL2000 [14].

2.8. Phasing, refinement and structure analysis

The structure of the substrate-free enzyme was solved to a resolution of 1.80 Å by molecular replacement using Phaser-MR [15] in the PHENIX program suite [16]. The structure of putative GABA-AT from *Sulfolobus tokodaii* strain7 (PDB ID: 2eo5; RIKEN Structural Genomics/Proteomics Initiative, unpublished work) served as the search model. Data in the resolution range 50-3 Å were used for the molecular replacement. The program DM [17] in the CCP4 program suite [18] was used for noncrystallographic symmetry (NCS) averaging and solvent flattening of the electron-density map. Model building was performed using the program Coot [19]. Maximum-likelihood refinement at 1.80 Å resolution was performed using REFMAC5 [20]. NCS restraints were imposed during initial refinement. Then after several cycles of inspection of the 2Fo-Fc and Fo-Fc density maps, the model was rebuilt. In the final refined model, $R = 0.173$ ($R_{free} = 0.202$).

The structure of the L-Orn-bound enzyme was solved to a resolution of 1.92 Å by molecular replacement using Phaser-MR [15]. As a search model, the structure of chain A from the substrate-free enzyme was used. Data in the resolution range 50-3 Å were used for the molecular replacement. The model was then rebuild using Coot [19], and refinement at the maximum resolution was performed using REFMAC5 [20] as described for the substrate-free enzyme. In the final model, $R = 0.181$ ($R_{free} = 0.215$). The structure of the PLP-L-Glu-bound enzyme was solved to a resolution of 2.99 Å. The molecular replacement, model building, and refinement were respectively performed using Phaser-MR [15], Coot [19], and REFMAC5 [20] as described for the L-Orn-bound enzyme. In the final model, $R = 0.220$ ($R_{free} = 0.284$).

In all cases, water molecules were incorporated using Coot [19], and model geometry was analyzed using MolProbity [21]. The data collection and refinement statistics are listed in Table 3. Hydrogen bonds were identified using CCP4mg [22]. For superposition of the structures, secondary-structure matching [23] was performed using Coot [19]. Molecular-graphics figures were created using PyMOL (http://www.pymol.org/). The final Fo - Fc omit electron density maps were generated using Polder Maps [24] in the PHENIX program suite [16]. The atomic coordinates and structure factors have been deposited in the Protein Data Bank (http://www.rcsb.org/; IDs: 7vno, 7vnt, and 7vo1).

3. Results and Discussion

3.1. Gene expression and enzyme purification

A recombinant Orn-AT was successfully produced in *Escherichia coli* and purified through heat treatment and Co^{2+}-chelating Sepharose chromatography. The purified enzyme showed a single band at about 50 kDa on SDS-PAGE (Supplementary Fig. 1A). Gel filtration chromatography showed the native molecular mass of the enzyme to be 197 kDa (Supplementary Fig. 1B), indicating the enzyme has a tetrameric structure.

We were unable to isolate the apo-form of the enzyme through heat treatment [10] or incubation with hydroxylamine hydrochloride. To prepare PLP-free Orn-AT, the heat treatment step was omitted from the purification, and the enzyme bound to the Co^{2+}-chelating Sepharose column was denatured with 4 M guanidine hydrochloride. Thereafter, the apo-enzyme was refolded as described in Experimental procedures. In the absence of PLP in the assay, the prepared apo-enzyme still exhibited the activity of 0.14 μmol/min/mg, which was markedly less than that (0.80 μmol/min/mg) of the purified holo-enzyme (the activity was assayed at 37°C to avoid the influence of the temperature). Apo-enzyme was successfully reconstituted with PLP by heating for 20 min at 80°C and the reconstituted-enzyme showed the activity of 1.36 μmol/min/mg, which was 1.7 times

higher than that of the normally purified holo-enzyme. The enzyme reconstituted with PLP-L-Glu exhibited the activity of 0.14 μmol/min/mg, which corresponds to 10 % of the activity of the enzyme reconstituted with PLP. These enzyme activities hardly increased in the assay with PLP (data not shown). The spectral analyses of these enzymes also support the correct reconstitution of the enzyme with PLP and PLP-L-Glu (Supplementary Fig. 2). PLP contents of the normally purified holo-enzyme and the PLP-reconstituted-enzyme were calculated to be 0.68 and 0.84 mol/mol of subunit, respectively. The activities of these enzymes were not changed when the enzymatic assays were performed in the presence of exogenous PLP (data not shown). These results suggest that PLP-unbounded enzyme which did not recover the activity by exogenous PLP is partially present in these recombinant enzymes.

3.2. Enzymatic properties of Orn-AT

The amino donor specificity of Orn-AT was determined using β-alanine, GABA, 5-aminovalerate, 6-aminohexanoate, 2,3-diaminopropionate, 2,4-diaminobutyrate, L-Orn, L-Lys, D-Orn and D-Lys as donors with 2-oxoglutarate as the amino acceptor. β-Alanine, 2,3-diaminopropionate, and 2,4-diaminobutyrate were inert as amino donors (Table 1). Aminotransferase activity was detected for L-Orn (100%), L-Lys (95%), 5-aminovalerate

(82%), 6-aminohexanoate (49%) and GABA (28%), indicating the enzyme predominantly catalyzes the transfer of δ- and ε-amino groups, irrespective of the presence of an α-amino group. In addition, the enzyme also exhibited activity toward the D-enantiomers D-Lys (88%) and D-Orn (19%). Next, the amino acceptor specificity was examined using 2-oxoglutarate, pyruvate, and oxaloacetate as acceptors with L-Orn as the amino donor. The enzyme activity was found to be specific for 2-oxoglutarate; pyruvate and oxaloacetate were inert (Table 1). These results coincide with those obtained with *T. kodakarensis* Orn-AT [8].

The enzyme's kinetics were assessed using various concentrations of L-Orn, L-Lys, D-Orn, and D-Lys with a constant concentration of 2-oxoglutarate, after which the kinetic parameters were calculated using a non-linear regression model (Table 2). The k_{cat} and K_m values for the amino donors revealed that L-Orn was the most preferable substrate for this enzyme. With L-Orn as the amino donor, the k_{cat}/K_m value for 2-oxoglutarate was also higher than with L-Lys, D-Orn, or D-Lys as the amino donor.

The optimum temperature and pH for the enzyme reaction were >90°C and pH 6.5-7.0, respectively. Enzyme activity was not lost after incubation at 80°C for at least 24 h or after incubation at 80°C for 30 min at pHs ranging from 4.0 to 10.5, which are typical features of hyperthermophilic enzymes.

3.3. Overall structure

The structure of *P. horikoshii* Orn-AT with PLP bound was determined using molecular replacement and refined to a resolution of 1.80 Å (Table 3). The asymmetric unit consisted of one homodimer with a solvent content of 53.4%, which corresponds to a Matthew's coefficient [25] of 2.64 $Å^3$ Da^{-1}. The crystal structure indicated that the quaternary structure of *P. horikoshii* Orn-AT was a dimer of dimers generated with a crystallographic twofold axis (Fig. 2A). Oligomerization-state analysis using Proteins, Interfaces, Structures and Assemblies (PISA) [26] confirmed the tetrameric arrangement of *P. horikoshii* Orn-AT, which is consistent with the subunit assembly of the enzyme as estimated using gel filtration and SDS-PAGE (native enzyme 197 kDa, subunit 50 kDa). The interface accessible surface areas (ASAs) were calculated to be about 5000 $Å^2$ and 1500 $Å^2$ for the subunit A-B and A-C interfaces, respectively.

The model of the dimer contained ordered residues 3 to 454 in subunits A and B, as well as two PLP molecules, two glycerol molecules, three ethylene glycol molecules and 641 water molecules. Each monomer consisted of three domains: an N-terminal domain (residues 3-59), a C-terminal domain (residues 343-454), and a large PLP-binding domain (residues 60-342) (Fig. 2B).

3.4. Comparison with the human Orn-AT structure

Superposition of the structure of human Orn-AT (Protein Data Bank (PDB) ID: 1oat, subunit A) onto that of *P. horikoshii* Orn-AT (PDB ID: 7vno, subunit A) yielded a root mean square deviation (r.m.s.d.) of 1.68 Å for the equivalent Cα atoms in 324 residues. Despite relatively low sequence identity (28%), the main-chain coordinates and secondary structure of the *P. horikoshii* Orn-AT monomer are basically the same as those of human Orn-AT: helix α1 and strands β1-β3 make up the N-terminal domain, helices α2-α9 and strands β4-β10 comprise the PLP-binding domain, and α10-α12 and β11-β14 form the C-terminal domain (Fig. 2B). However, a clear topological difference was observed in the length and/or position of several surface loops in the two enzymes (Fig. 2C). Loops L1, L2, and L3 in *P. horikoshii* Orn-AT, which are composed of residues 185-200, 383-391, and the C-terminal residues 445-454, respectively, were markedly larger than the corresponding loops in human Orn-AT. Moreover, the positioning of these loops largely differs between the two enzymes. Further, residues 158-166 (L4) in the human enzyme are absent from the corresponding loop region of *P. horikoshii* Orn-AT. Among the loops L1, L2, and L3 in *P. horikoshii* Orn-AT, L1 in subunit A is closely associated with the same loop in subunit C. In that region, we observed a large hydrophobic cluster

composed of 10 residues [Pro183, Pro191 (L1), Trp192 (L1), Tyr210, and Tyr214 in both subunits (Supplementary Fig. 3)], which are not observed in human enzyme. The human Orn-AT (holo-form) has been reported to have an apparent T_m value of 67°C [27]. The presence of the strong intersubunit hydrophobic interactions in this region may be involved in the higher thermal stability of the *P. horikoshii* Orn-AT.

The quaternary structure of human Orn-AT was estimated to be a hexamer (a trimer of dimers), based on analysis of the packing of the monomer within the crystal [6]. However, recombinant human Orn-AT was found to be a tetrameric structure with a tetramer-dimer equilibrium in solution [27]. Because a dimeric structure similar to human Orn-AT is seen within the tetrameric structure of *P. horikoshii* Orn-AT, the both enzymes may have the same subunit assembly (tetramer).

3.5. Comparison of the PLP- and L-Orn-binding sites

The structure of the L-Orn/PLP-bound enzyme was refined to a resolution of 1.92 Å. This is the first structure of an Orn-AT in complex with its natural substrate. In the initial electron-density map, an extra density in addition to the density for PLP was observed within the active-site cavity of one subunit (subunit A) of the dimer; no such density was detected in the other subunit (subunit B). After refinement of the peptide chain, L-Orn

could be modelled into that density (Fig. 3B). The final model (dimer) of the L-Orn/PLP-bound enzyme (PDB ID: 7vnt) was composed of amino-acid residues 3-454 in each subunit, one L-Orn molecule, two PLP molecules, one glycerol molecule, one ethylene glycol molecule, and 564 water molecules. The two subunits in this model were nearly identical, with a backbone r.m.s.d. of 0.19, though the bound L-Orn was detected only in one subunit within the dimer. Thus, the movement of domain that accompanies substrate binding was not observed in *P. horikoshii* Orn-AT. Because the PLP-L-Orn Shiff base linkage is visible in the electron density map, a proper external aldimine is thought to be formed in the active site. When we superimposed the structure of PLP-L-Glu-bound enzyme onto the substrate-free enzyme structure, notable domain movement was not observed (a backbone r.m.s.d. of 0.23, data not shown). This suggests that the binding of the substrate does not give rise to a large structural change around the active site. The reason for the presence of the substrate in only one active site is still not clear.

The crystal structure of human Orn-AT (PDB ID: 2oat) in complex with the inhibitor 5-fluoromethylornitine (FMO) has been reported previously [28]. When we superimposed that structure onto the structure of L-Orn/PLP-bound *P. horikoshii* Orn-AT, we found that the direct interactions between the PLP molecule and the enzyme protein are completely conserved between the two enzymes (Supplementary Fig. 4). Briefly, in

P. horikoshii Orn-AT, the phosphoryl group interacts with the backbone N atom of Gly124 (Gly142 in human Orn-AT), the backbone N atom of Thr125 (Val143 in human Orn-AT), and the side-chain O and backbone N atoms of Thr321* (Thr322* in human Orn-AT) (the asterisk indicates a residue in the neighboring subunit within the dimer). The O3 atom of PLP interacts with the side chain of Gln267 (Gln266 in human Orn-AT). The pyridine N atom of PLP makes a salt bridge with the side chain of Asp264 (Asp263 in human Orn-AT). Although Thr125 was replaced by Val143 in human Orn-AT, the backbone amide of Val143 is situated at a position where it can interact with the phosphoryl group of PLP, as Thr125 does. Within the substrate-free *P. horikoshii* Orn-AT structure, the C4 atom of PLP binds covalently to the side chain of Lys293 (Lys292 in human Orn-AT) to form an internal aldimine linkage.

Based on the structure of inhibitor-bound human Orn-AT, the natural substrate L-Orn has been modeled into the active site as an external aldimine intermediate [28]. In that model, the main residues responsible for the specific binding of L-Orn were thought to be Tyr55 and Arg180; the former is likely involved in a hydrogen bond with the α-amino group and the latter forms a salt bridge with the α-carboxylate (Fig. 3A, the human Orn-AT active site with inhibitor bound is indicated). In addition, the two aromatic residues, Tyr85 and Phe177, were observed to form a hydrophobic sandwich that accommodates

the side chain of L-Orn. On the other hand, mutation analysis of human Orn-AT suggests that Tyr85 is a major determinant of specificity toward L-Orn [29]; Y85I mutation greatly decreased the reaction rate of the enzyme with L-Orn (1/1000), but increased that with GABA (16-fold), which lacks the α-amino group. Because the α-amino group of L-Orn is held between the OH groups of Tyr55 and Tyr85, both of those residues are likely responsible for the suitable binding of L-Orn. Within our model, Arg180 and Phe177 in human Orn-AT were respectively conserved as Arg154 and Phe151 in *P. horikoshii* Orn-AT, whereas the residues corresponding to Tyr55 and Tyr85 were replaced by Thr30 and Ile63, respectively (Fig. 3B). Although the side chain of Ile63 forms hydrophobic interactions with the side chain of L-Orn, no interaction was observed between Thr30 and the substrate. Instead, the side chains of Thr92* and Asp93*, which arise from a loop (residues 90-94) in the neighboring subunit (subunit B), form hydrogen bonds with the α-amino group of L-Orn (Fig. 3B). The residues involved in the corresponding loop in human Orn-AT have no interactions with the substrate. These observations mean that the manner by which the α-amino group of L-Orn is recognized totally differs between the two enzymes.

To assess the roles of Thr92* and Asp93*, we constructed T92V and D93L mutants. These substitutions were selected because the size of the side chains of Val and Leu are

similar to those of Thr and Asp, respectively. We observed that the D93L substitution reduces the specific activity of the mutant enzyme (V_{max}: 2.1 μmol/min/mg) compared to the wild-type enzyme (V_{max}: 4.9 μmol/min/mg). The specific activity of the T92V mutant (V_{max}: 6.2 μmol/min/mg) was slightly higher than that of the wild-type enzyme. In both mutants, the K_m values for L-Orn (0.28 mM for T92V and 1.2 mM for D93L) were higher than that (0.11 mM) of the wild-type enzyme. However, the K_m value of T92V is only 3-fold higher than that of the wild-type enzyme. Multiple sequence alignment (Supplementary Fig. 5) showed that Asp93 was completely conserved among the enzymes belonging to the Orn-AT group (group 3: see below) [10] of archaeal GABA-AT homologues. In contrast, the residues corresponding Thr92 were conserved as Thr or replaced by Asn. These results suggest a minimal involvement of the Thr92* in the substrate binding. In addition, the V_{max} value of the D93L mutant was not drastically reduced compared to that of the wild-type enzyme. Therefore, it is still unclear whether Asp93* is a major contributor to the suitable binding of L-Orn, though Asp93* is thought to play critical roles in maintaining high affinity for the substrate. Because the selected substitutions completely abolish the polarity of the original residues, much larger structural alteration might occur in the active site of the mutant. Further investigation is required to verify the role of the Asp93*.

3.6. Structural demonstration of the "Glu switch" mechanism

Within the active site of the L-Orn-bound model of human Orn-AT [28], the side chain of Arg413 is covered by the side chain of Glu235, and the α-carboxylate of L-Orn binds to the side chain of Arg180 (Fig. 4A; the active site of inhibitor-bound human Orn-AT is indicated). Therefore, a "Glu235 switch" mechanism that prevents L-Orn from binding in an orientation that would lead to transamination of the α-amino group has been proposed [28]. In that mechanism, the function of Glu235 is thought to be to neutralize the positive charge of Arg413 when L-Orn binds to the active site. In the second half-reaction, the side chain of Glu235 is supposed to switch its position, uncovering Arg413, thereby enabling the Arg413 side-chain to interact with the α-carboxylate of 2-oxoglutarate or L-Glu. This hypothesis was subsequently tested in a mutational analysis of human Orn-AT [29]. It was observed that the E235A mutant retained its regiospecificity for the ω-amino group of L-Orn, but the L-Glu reaction was enhanced 650-fold, whereas the 2-oxoglutarate reaction rate was enhanced only a 5-fold. Therefore, a modified mechanism was proposed in which the Glu235 switch is closed in the pyridoxaldimine form of the enzyme, which allows suitable binding of L-Orn but impedes binding of L-Glu, and is open in the pyridoxamine form, making Arg413 available to bind 2-oxoglutarate [29].

Within the *P. horikoshii* Orn-AT structure, Glu235 and Arg413 in human Orn-AT are conserved as Glu236 and Arg419, respectively. In the L-Orn-bound *P. horikoshii* Orn-AT, the side-chain of Glu236 forms a salt bridge with that of Arg419, closing the "Glu switch" and thus preventing unsuitable L-Orn binding (Fig. 4B).

To test the "Glu switch" hypothesis, we performed a crystal structure analysis of the PLP-L-Glu-bound enzyme. The structure was refined to a resolution of 2.99 Å. The final model (dimer) of the PLP-L-Glu enzyme (PDB ID: 7vo1) was composed of amino-acid residues 3-454 in each subunit, two PLP-L-Glu molecules, and 29 water molecules. Although the electron density for the covalent bond connecting the Cα atom of L-Glu and the pyridine ring of PLP was discontinuous, the significant electron density at the L-Glu and PLP moieties enabled us to deduce a plausible structure for PLP-L-Glu (Fig. 4C). In this model, we found that the side-chain of Glu236 rotates clockwise by about 56° around the Cβ atom of Glu236 relative to the L-Orn-bound *P. horikoshii* Orn-AT structure. As a result, the side-chain carboxylate of Glu236 faces in the direction opposite to the side-chain of Arg419. Instead, the α-carboxylate of the L-Glu moiety in PLP-L-Glu interacts with the side-chain of Arg419. These observations clearly indicate that the "Glu switch" functions in this archaeal Orn-AT. Moreover, the *P. horikoshii* Orn-AT structure in complex with the external aldimine PLP-L-Glu adduct provides the first structural

evidence for a “Glu switch” mechanism.

We previously reported that the GABA-AT homologues in the *Pyrococcus* and *Thermococcus* strains in the genome database are divided into four groups (group 1, 2, 3, and 4, which are respectively represented by the PH0138, PH0782, PH1423, and PH1501 gene products) [9, 30]. The clade that includes these 4 groups harbored many uncharacterized proteins. Our recent studies revealed that groups 1, 2, 3, and 4 include broad substrate specificity amino acid racemase (BAR), alanine- and serine-specific racemase (ASR), Orn-AT, and racemase with moderate substrate specificity (MAR), respectively [9, 10, 30, 31]. The present study describes the first structure of a novel type of Orn-AT belonging to group 3, and our results may provide critical information that will facilitate better understanding of the structure-function relationships within archaeal GABA-AT homologues.

4. Conclusions

We showed that the putative GABA-AT gene of *P. horikoshii* expressed in *E. coli* cells produces an enzyme exhibiting Orn-AT activity. We successfully determined the crystal structure of the enzyme and its structure-function relationship with regard to substrate binding. The substrate recognition residues were found to be

notably different from those of human Orn-AT. Moreover, the structure in complex with the external aldimine provides the first structural evidence for a “Glu switch” mechanism in the dual substrate specificity of Orn-AT. Our findings on the crystal structure of this novel archaeal ω-aminotransferase will facilitate better understanding of the structure-function relationships within archaeal GABA-AT homologues.

The following is the supplementary data related to this article.

Supplementary Table 1.

Primer sequences for site-directed mutagenesis.

Supplementary Fig. 1.

A, SDS-PAGE of the purified *P. horikoshii* Orn-AT.

B, Calibration curve of gel filtration chromatography.

Supplementary Fig. 2

Spectral analyses of *P. horikoshii* Orn-ATs.

Supplementary Fig. 3

Intersubunit (A - C) hydrophobic cluster formed by 10 residues in *P. horikoshii* Orn-AT.

Supplementary Fig. 4.

Comparison of the PLP-binding site structures in *P. horikoshii* Orn-AT (green and black labels) and human Orn-AT. (cyan and red labels) (stereo representation).

Supplementary Fig. 5.

Multiple alignment analysis of the primary structures of the archaeal Orn-ATs.

Acknowledgments

We are grateful to the staff of the Photon Factory for their assistance with data collection, which was approved by the Photon Factory Program Advisory Committee. This work was supported in part by research funds from the Public Utility Foundation for the Vitamin & Biofactor Society (to H. S.) and the Japan Society for the Promotion of Science (KAKENHI grant No. 18H02138 to H. S., 20K05729 to R.K., and 20K05816 to To. O.).

Footnotes

The abbreviations used are: Orn-AT, ornithine δ-aminotransferase; L-Orn, L-ornithine; L-Glu, L-glutamate; PLP, pyridoxal 5'-phosphate; PLP-L-Glu, *N*-(5'-phosphopyridoxyl)-L-glutamate; P5C, L-1-pyrroline-5-carboxylate; GABA-AT, γ-aminobutyrate aminotransferase; BAR, broad substrate specificity amino acid racemase; ASR, alanine

and serine specific racemase; MAR, moderate substrate specificity amino acid racemase; PDB, Protein Data Bank; ASA, accessible surface area; r.m.s.d., root-mean-square deviation; FMO, 5-fluoromethylornitine.

Author contributions

HS supervised the project; RK, TaO, and JH performed crystallographic experiments; HS and TaO performed data collection and model building; RK performed biochemical assays and UPLC analyses; TF performed NMR analysis; RK, KY, ToO, JH, and HS analyzed data and prepared the manuscript. All authors had approved the submitted and published version of the manuscript.

Conflict of interest

The authors declare no conflicts of interest.

Ethical statement

This article does not contain any studies with human participants or animals performed by any of the authors.

References

[1] K. Yonaha, M. Nishie, S. Aibara, The primary structure of ω-amino acid:pyruvate aminotransferase, J. Biol. Chem. 267(18) (1992) 12506-12510.

[2] C. Rausch, A. Lerchner, A. Schiefner, A. Skerra, Crystal structure of the ω-aminotransferase from *Paracoccus denitrificans* and its phylogenetic relationship with other class III aminotransferases that have biotechnological potential, Proteins 81 (2013) 774-787.

[3] A. Sarup, O.M. Larsson, A. Schousboe, GABA transporters and GABA-transaminase as drug targets, Curr. Drug Targets CNS Neurol. Disord. 2 (2003) 269-277.

[4] G. Daune, N. Seiler, Interrelationships between ornithine, glutamate, and GABA. II. Consequences of inhibition of GABA-T and ornithine aminotransferase in brain, Neurochem. Res. 13 (1988) 69-75.

[5] J.J. O'Donnell, R.P. Sandman, S.R. Martin, Gyrate atrophy of the retina: inborn error of L-ornithin:2-oxoacid aminotransferase, Science 200 (1978) 200-201.

[6] B.W. Shen, M. Hennig, E. Hohenester, J.N. Jansonius, T. Schirmer, Crystal structure of human recombinant ornithine aminotransferase, J. Mol. Biol. 277 (1998) 81-102.

[7] J.A. Williams, G. Bridge, L.J. Fowler, R.A. John, The reaction of ornithine aminotransferase with ornithine, Biochem. J. 201 (1982) 221-225.

[8] R.C. Zheng, S.I. Hachisuka, H. Tomita, T. Imanaka, Y.G. Zheng, M. Nishiyama, H. Atomi, An ornithine ω-aminotransferase required for growth in the absence of exogenous proline in the archaeon *Thermococcus kodakarensis*, J. Biol. Chem. 293 (2018) 3625-3636.

[9] R. Kawakami, C. Kinoshita, T. Kawase, M. Sato, J. Hayashi, H. Sakuraba, T. Ohshima, Characterization of a novel moderate-substrate specificity amino acid racemase from the hyperthermophilic archaeon *Thermococcus litoralis*, Biosci. Biotechnol. Biochem. 85 (2021) 1650-1657.

[10] R. Kawakami, T. Ohshida, H. Sakuraba, T. Ohshima, A novel PLP-dependent alanine/serine racemase from the hyperthermophilic archaeon *Pyrococcus horikoshii* OT-3, Front. Microbiol. 9 (2018) 1481.

[11] R. Voellmy, T. Leisinger, Dual role for *N*-2-acetylornithine 5-aminotransferase from *Pseudomonas aeruginosa* in arginine biosynthesis and arginine catabolism, J. Bacteriol. 122 (1975) 799-809.

[12] J.C. Fothergill, J.R. Guest, Catabolism of L-lysine by *Pseudomonas aeruginosa*, J. Gen. Microbiol. 99 (1977) 139-155.

[13] J. Hayashi, Y. Mutaguchi, Y. Minemura, N. Nakagawa, K. Yoneda, T. Ohmori, T. Ohshima, H. Sakuraba, Crystal structure of the novel amino-acid racemase isoleucine 2-

epimerase from *Lactobacillus buchneri*, Acta crystallogr. D, Biol. Crystallogr. 73 (2017) 428-437.

[14] Z. Otwinowski, W. Minor, Processing of X-ray diffraction data collected in oscillation mode, Methods Enzymol. 276 (1997) 307-326.

[15] A.J. McCoy, R.W. Grosse-Kunstleve, P.D. Adams, M.D. Winn, L.C. Storoni, R.J. Read, Phaser crystallographic software, J. Appl. Crystallogr. 40 (2007) 658-674.

[16] P.D. Adams, P.V. Afonine, G. Bunkoczi, V.B. Chen, I.W. Davis, N. Echols, J.J. Headd, L.W. Hung, G.J. Kapral, R.W. Grosse-Kunstleve, A.J. McCoy, N.W. Moriarty, R. Oeffner, R.J. Read, D.C. Richardson, J.S. Richardson, T.C. Terwilliger, P.H. Zwart, PHENIX: a comprehensive Python-based system for macromolecular structure solution, Acta Crystallogr. D Biol. Crystallogr. 66 (2010) 213-221.

[17] K.D. Cowtan, P. Main, Phase combination and cross validation in iterated density-modification calculations, Acta Crystallogr. D Biol. Crystallogr. 52 (1996) 43-48.

[18] M.D. Winn, C.C. Ballard, K.D. Cowtan, E.J. Dodson, P. Emsley, P.R. Evans, R.M. Keegan, E.B. Krissinel, A.G. Leslie, A. McCoy, S.J. McNicholas, G.N. Murshudov, N.S. Pannu, E.A. Potterton, H.R. Powell, R.J. Read, A. Vagin, K.S. Wilson, Overview of the CCP4 suite and current developments, Acta Crystallogr. D Biol. Crystallogr. 67 (2011) 235-242.

[19] P. Emsley, B. Lohkamp, W.G. Scott, K. Cowtan, Features and development of Coot, Acta Crystallogr. D Biol. Crystallogr. 66 (2010) 486-501.

[20] G.N. Murshudov, P. Skubak, A.A. Lebedev, N.S. Pannu, R.A. Steiner, R.A. Nicholls, M.D. Winn, F. Long, A.A. Vagin, REFMAC5 for the refinement of macromolecular crystal structures, Acta Crystallogr. D Biol. Crystallogr. 67 (2011) 355-367.

[21] S.C. Lovell, I.W. Davis, W.B. Arendall, 3rd, P.I. de Bakker, J.M. Word, M.G. Prisant, J.S. Richardson, D.C. Richardson, Structure validation by Cα geometry: ϕ, ψ and Cβ deviation, Proteins 50 (2003) 437-450.

[22] S. McNicholas, E. Potterton, K.S. Wilson, M.E. Noble, Presenting your structures: the CCP4mg molecular-graphics software, Acta Crystallogr. D Biol. Crystallogr. 67 (2011) 386-394.

[23] E. Krissinel, K. Henrick, Secondary-structure matching (SSM), a new tool for fast protein structure alignment in three dimensions, Acta Crystallogr. D Biol. Crystallogr. 60 (2004) 2256-2268.

[24] D. Liebschner, P.V. Afonine, N.W. Moriarty, B.K. Poon, O.V. Sobolev, T.C. Terwilliger, P.D. Adams, Polder maps: improving OMIT maps by excluding bulk solvent, Acta crystallogr. D Biol. Crystallogr. 73 (2017) 148-157.

[25] B.W. Matthews, Solvent content of protein crystals, J. Mol. Biol. 33 (1968) 491-497.

[26] E. Krissinel, K. Henrick, Inference of macromolecular assemblies from crystalline state, J. Mol. Biol. 372 (2007) 774-797.

[27] R. Montioli, C. Zamparelli, C. Borri Voltattorni, B. Cellini, Oligomeric state and thermal stability of apo- and holo- human ornithine δ-aminotransferase, Protein J. 36 (2017) 174-185.

[28] P. Storici, G. Capitani, R. Muller, T. Schirmer, J.N. Jansonius, Crystal structure of human ornithine aminotransferase complexed with the highly specific and potent inhibitor 5-fluoromethylornithine, J. Mol. Biol. 285 (1999) 297-309.

[29] M. Markova, C. Peneff, M.J. Hewlins, T. Schirmer, R.A. John, Determinants of substrate specificity in ω-aminotransferases, J. Biol. Chem. 280 (2005) 36409-36416.

[30] R. Kawakami, T. Ohmori, H. Sakuraba, T. Ohshima, Identification of a novel amino acid racemase from a hyperthermophilic archaeon *Pyrococcus horikoshii* OT-3 induced by D-amino acids, Amino Acids 47 (2015) 1579-1587.

[31] R. Kawakami, H. Sakuraba, T. Ohmori, T. Ohshima, First characterization of an archaeal amino acid racemase with broad substrate specificity from the hyperthermophile *Pyrococcus horikoshii* OT-3, J. Biosci. Bioeng. 124 (2017) 23-27.

Figure legends

Fig. 1. The two half-transamination reactions catalyzed by Orn-AT. E-PLP: pyridoxal form of the enzyme, E-PMP: pyridoxamine form of the enzyme.

Fig. 2. *A*, overall structure of the *P. horikoshii* Orn-AT tetramer with subunits shown in different colors (*left*). An image from a different angle (*right*) is shown. *B*, Ribbon plot of the *P. horikoshii* Orn-AT monomer. The N-terminal domain (residues 3-59), PLP-binding domain (residues 60-342) and C-terminal domain (residues 343-454) are in red, green and blue, respectively. The PLP molecule is shown in magenta. *C*, superposition of the structures of *P. horikoshii* Orn-AT (green) and human Orn-AT (yellow). The surface elements in *P. horikoshii* Orn-AT (L1, L2 and L3: blue) and those in human Orn-AT (L4: red) are shown.

Fig. 3. *A*, stereographic close-up of FMO bound to human Orn-AT. Residues that interact with FMO are shown in cyan. FMO and PLP are shown in yellow. *B*, stereographic close-up of L-Orn bound to *P. horikoshii* Orn-AT. Residues that interact with L-Orn are shown in green. L-Orn and PLP are shown in yellow. The final Fo - Fc omit electron density map

for L-Orn and PLP was generated using Polder Maps [24] (contoured at 3.5σ). The networks of hydrogen bonds are shown as dashed lines. Oxygen, phosphate and nitrogen atoms are shown in red, orange and blue, respectively.

Fig. 4. *A*, stereo representation of FMO bound to human Orn-AT. Residues that contribute to the "Glu switch" mechanism are shown in cyan. FMO and PLP are shown in yellow. *B*, stereo representation of L-Orn bound to *P. horikoshii* Orn-AT. Residues that contribute to the "Glu switch" mechanism are shown in green. L-Orn and PLP are shown in yellow. The final Fo - Fc omit electron density map for L-Orn, PLP and nearby residues was generated as in Figure 3B (contoured at 3.5σ). *C*, stereo representation of PLP-L-Glu bound to *P. horikoshii* Orn-AT. Residues that contribute to the "Glu switch" mechanism are shown in green. The final Fo - Fc omit electron density map for PLP-L-Glu and nearby residues was generated as in Figure 3B (contoured at 3.0σ). Oxygen, phosphate and nitrogen atoms are shown in red, orange and blue, respectively. The networks of hydrogen bonds are shown as dashed lines.

Supplementary Figure 1.
A, SDS-PAGE of the purified *P. horikoshii* Orn-AT. Lane 1, Wild type; lane 2, PLP-free apoenzyme; lane 3, molecular mass standard; lane 4, T92V mutant; lane 5, D93L mutant. Molecular masses (kDa) of the standards were displayed in the left side of the gel. *B*, Calibration curve of gel filtration chromatography. *P. horikoshii* Orn-AT was shown in square. The elution profile of the wild type enzyme was inserted.

A

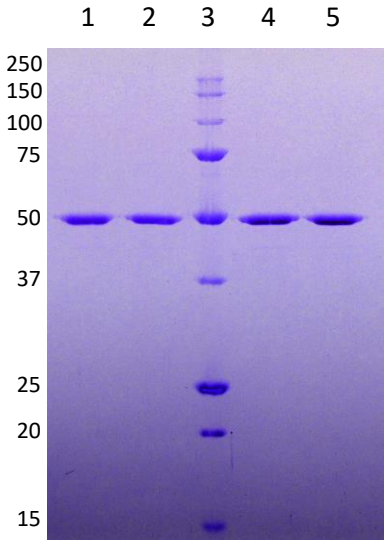

B

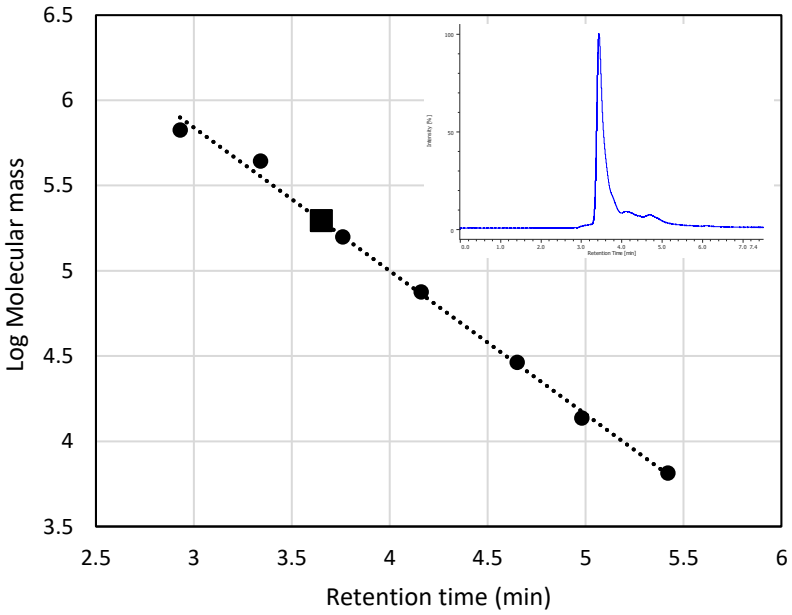

Supplementary Figure 2.
Spectral analyses of *P. horikoshii* Orn-ATs. Apo-enzyme, holo-enzyme, and the reconstituted enzyme with PLP and PLP-L-Glu were represented by black, red, blue, and green lines, respectively. The spectral data were corrected by the absorbance at 280 nm as 1.0.

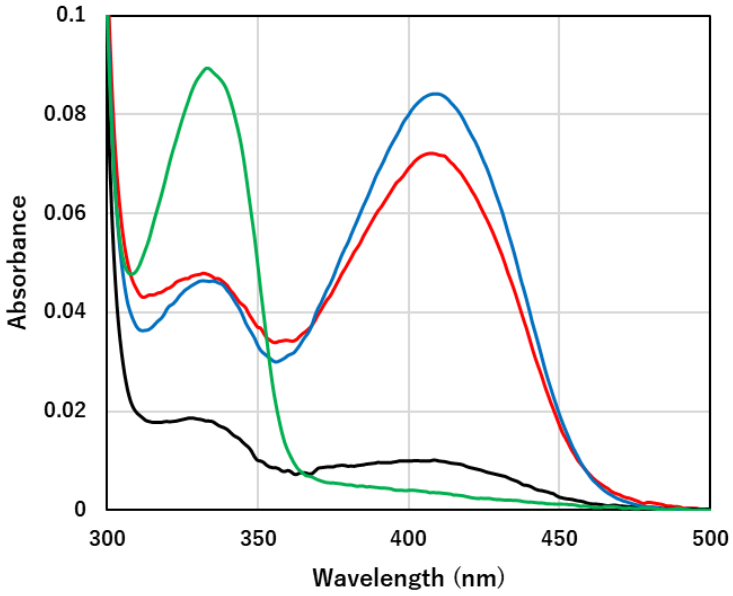

Supplementary Figure 3.

Intersubunit (A – C) hydrophobic cluster formed by 10 residues in *P. horikoshii* Orn–AT. The loop L1 is shown in blue. The residues belong to subunits A and C are shown in yellow and cyan, respectively.

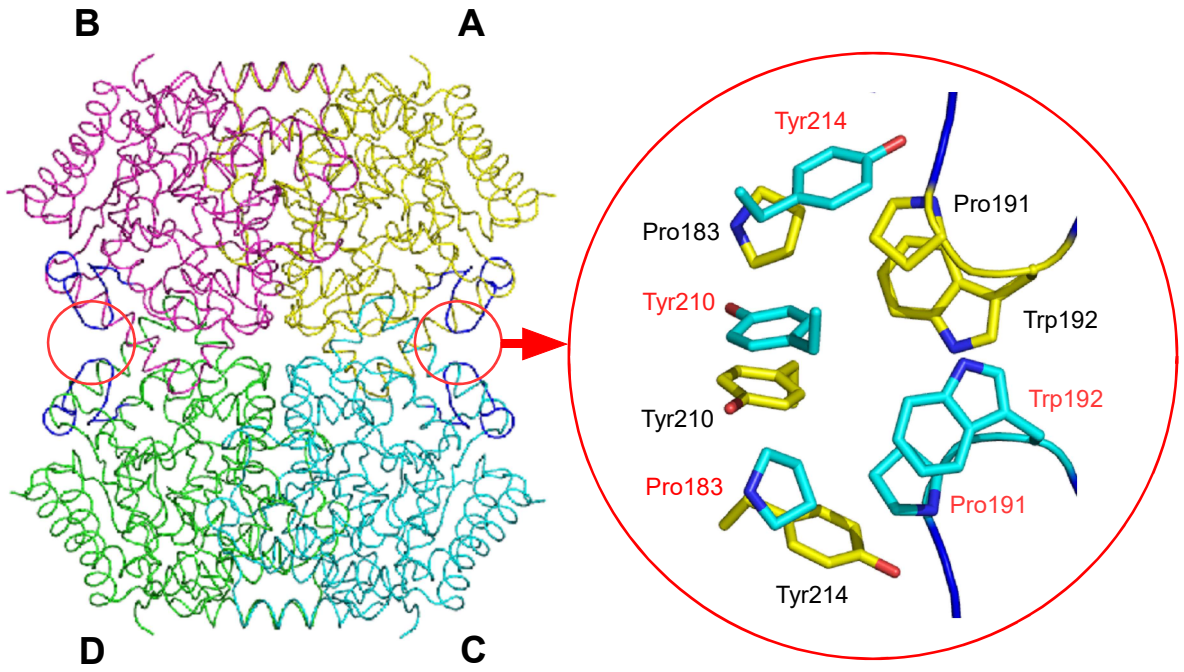

Supplementary Figure 4.

Comparison of the PLP-binding site structures in *P. horikoshii* Orn-AT (green and black labels) and human Orn-AT. (cyan and red labels) (stereo representation).

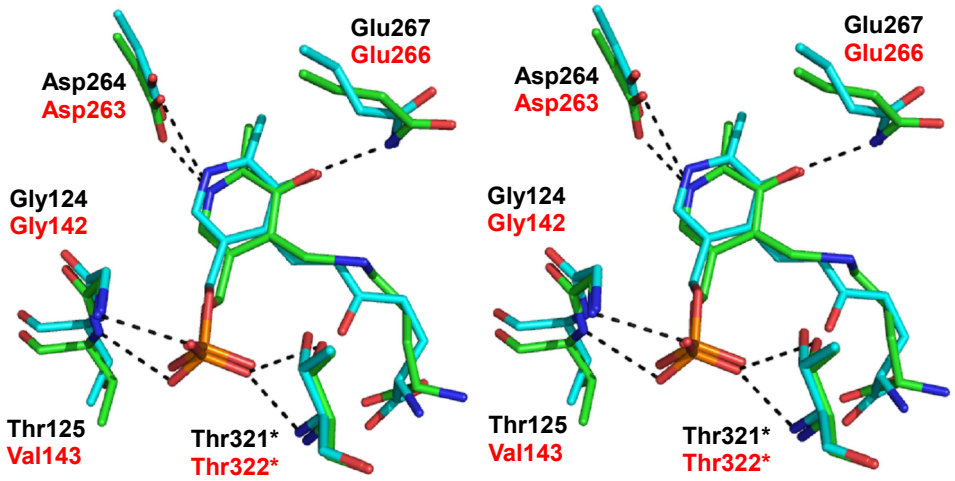

Supplementary Figure 5.

Multiple alignment analysis of the primary structures of the archaeal Orn-ATs. The primary structures in group 3 of GABA-ATs (9) were aligned using ClustalW program. The residues 92 and 93 were boxed in red. Abbreviations are as follows: thh, *Thermococcus* sp. 5-4; trl, *T. radiotolerans*; the, *Thermococcus* sp. 4557; tbs, *T. barossii*; thm, *T. cleftensis*; tpaf, *T. pacificus*; ttd, *T. thioreducens*; ton, *T. onnurineus*; tpie, *T. piezophilus*; tce, *T. celer*; thy, *Thermococcus* sp. P6; teu, *T. eurythermalis*; tgy, *T. guaymasensis*; tba, *T. barophilus*; ths, *T. paralvinellae*; ppac, *Palaeococcus pacificus*; tko, *T. kodakarensis*; tgg, *T. gorgonarius*; tpep, *T. peptonophilus*; tsl, *T. siculi*; tprf, *T. profundus*; tga, *T. gammatolerans*; tha, *Thermococcus* sp. AM4; tnu, *T. nautili*; pfu, *P. furiosus*; pya, *P. yayanosii*; pho, *P. horikoshii*; pab, *P. abyssi*; pyn, *Pyrococcus* sp. NA2; pyc, *P. kukulkanii*; tch, *T. chitonophagus*; pys, *Pyrococcus* sp. ST04; tlt, *T. litoralis*; thv, *Thermococcus* sp. 2319 × 1; and tsi, *T. sibiricus.*

```
thh_CDI07_08835      61 SGVGVLNVGHAHPRVVEAVKRQAEKFTHFALNDFFYENAVILAQKLAEISPGDFPKKVVY 120
trl_A3L10_08330      61 SGVGVLNVGHAHPRVVKAVKRQAEKFTHFALNDFFYENAIVLANKLAELAPGDFPKKVVY 120
the_GQS_07400        61 SGVGVLNVGHAHPRVVEAVKRQAEKFTHFALNDFFYENAVILAQKLAELAPGDFPKKVVY 120
tbs_A3L01_08850      61 SGVGVLNVGHAHPRVVEAIKRQSEKFTHFALNDFFYENAVVLAQKLAELSPGDFPKKVVY 120
thm_CL1_1122         61 SGVGVLNVGHAHPRVVEAIKRQAEKFTHFALNDFFYENAIVLANKLAELAPGDFPKKVVY 120
tpaf_A3L08_01845     61 SGVGVLNVGHAHPRVVEAVKRQAEKFTHFALNDFFYENAVILAQKLAELAPGDFPKKVVY 120
ttd_A3L14_11435      61 SGVGVLNVGHTHPRVVEAIKRQAEKFTHFALNDFFYENAITLANKLAELAPGDFPKKVVY 120
ton_TON_1605         61 SGVGVLNVGHAHPRVVEAVKKQAEKFTHFALNDFFYENAIILANKLAELAPGDFPKKVVY 120
tpie_A7C91_04125     61 SGVGVLNVGHVHPRVVEAVKRQAEKFTHFALNDFFYENAVILAQKLAELAPGDFPKKVVY 120
tce_A3L02_07860      61 SGVGVLNVGHAHPRVVEAIKRQAEKFTHFALNDFFYENAVILAGKLAELTPGDFQKKVVY 120
thy_A3L12_04555      60 SGVGVLNVGHAHPRVVEAIKRQAERFTHFALNDFFYENAIILANKLAELAPGDFKKKVVY 119
teu_TEU_02055        61 SGVGVLNVGHTHPRVVEAIKRQAEKFTHFALNDFFYENAVILANKLAELAPGDFPKKVVY 120
tgy_X802_04845       61 SGVGVLNVGHAHPRVVEAIKRQAEKFTHFALNDFFYENAVILANKLAELAPGDFPKKVVY 120
tba_TERMP_01538      61 SGVGVLNVGHVHPRVIEAIKRQAEKFTHFALNDFFYENAVILAQKLAELSPGDFPKKVVY 120
ths_TES1_1534        61 SGVGVLNVGHTHPRVIEAIKKQAEKFTHFALNDFFYENAVILAQKLAELSPGEFPKKVVY 120
ppac_PAP_04390       61 SGVGVMNVGHAHPKVVEAVKRQAEKFTHFALNDFFYENAVVLAQKLSELAPGDFAKKVAY 120
tko_TK2101           61 SGVGVINVGHSHPRVVEAIKKQAEKFTHYSLTDFFYENAIILAEKLIELAPGDIERKVVY 120
tgg_A3K92_08800      61 SGVGVINVGHSHPRVIEAIKKQVEKFTHYSLTDFFYENAIILAEKLIELAPGDMERKVVY 120
tpep_A0127_05395     61 SGVGVINVGHAHPRVVEAIKKQAEKFTHYSLTDFFYENAVVLAEKLIELAPGDIERKVVY 120
tsl_A3L11_02335      61 SGVGVINVGHAHPRVVEAIKKQAEKFTHYSLTDFFYENAVVLAEKLIELAPGDFEKKVVY 120
tprf_A3L09_01030     61 SGVGVINVGHSHPRVVEAIKKQAEKFTHYSLTDFFYENAVVLAEKLIELAPGDFEKKVVY 120
tga_TGAM_0179        61 SGVGVINVGHAHPRVVEAIKKQAEKFTHYSLTDFFYENAVVLAEKLIELAPGDFEKKVVY 120
tha_TAM4_1269        61 SGVGVINVGHAHPRVVEAIKKQAEKFTHYSLTDFFYENAVVLAEKLIELAPGDFEKKVVY 120
tnu_BD01_1869        61 SGVGVINVGHAHPRVVEAIKKQAEKFTHYSLTDFFYENAVILAEKLIELAPGDFEKKVVY 120
pfu_PF1421           61 SGIGVLNVGLRNPRVVEAIKKQLDLVLHAAGTDYYNPYQVALAEKLVQITPGDFEKKVFL 120
pya_PYCH_10940       61 SGIGVMNVGLRNPKVVEAVKKQLELVLHAAGTDYYNPYQVALAEKLVQITPGDFEKKVFL 120
pho_PH1423           61 SGIGVMNVGLRNPKVIEAIKKQLDLVLHAAGTDYYNPYQVELAKKLVEIAPGDIERKVFL 120
pab_PAB0501          61 SGIGVMNVGLRNPKVIEAIKKQLDLVLHAAGTDYYNPYQVELAKKLIEIAPGDMERKVFL 120
pyn_PNA2_0013        61 SGIGVMNVGLRNPKVIEAIKRQLDLVLHAAGTDYYNPYQVELAKKLAEIAPGDVERKVFL 120
pyc_TQ32_09735       61 SGIGVMNVGLRNPKVIEAIKKQLDLVLHAAGTDYYNPYQVELAKKLVEIAPGDVERKVFL 120
tch_CHITON_1656      61 SGIGVMNVGLRNPKVIEAIKKQLDLVLHAAGTDYYNPYQVELAKKLAEIAPGDVERKVFL 120
pys_Py04_1327        61 SGIGVMNVGLRNPKVIEAIKKQLDLVLHAAGTDYYNPYQVELAKKLAEIAPGDVERKVFL 120
tlt_OCC_00582        61 SGIGVLNAGLRNPRVVEALKEQLDKLIHGAGTDYYNPYQVALAEKLDSIAPGDFEKKTFL 120
thv_ADU37_CDS13120   61 SGIGVLNVGLRNPKVVEALKEQLDKVIHAAGTDYYNPYQVALAEKLDSIAPGDFEKKTFL 120
tsi_TSIB_1150        61 SGIGVLNAGLRNPRLVEALKKQLDKLIHGAGTDYYNPYQVALVEKLDSIAPGDFEKKTFL 120
                           **:**:*.*  :*::::*:*.* : . * : .*::    : *. ** .::**:. :*.
```

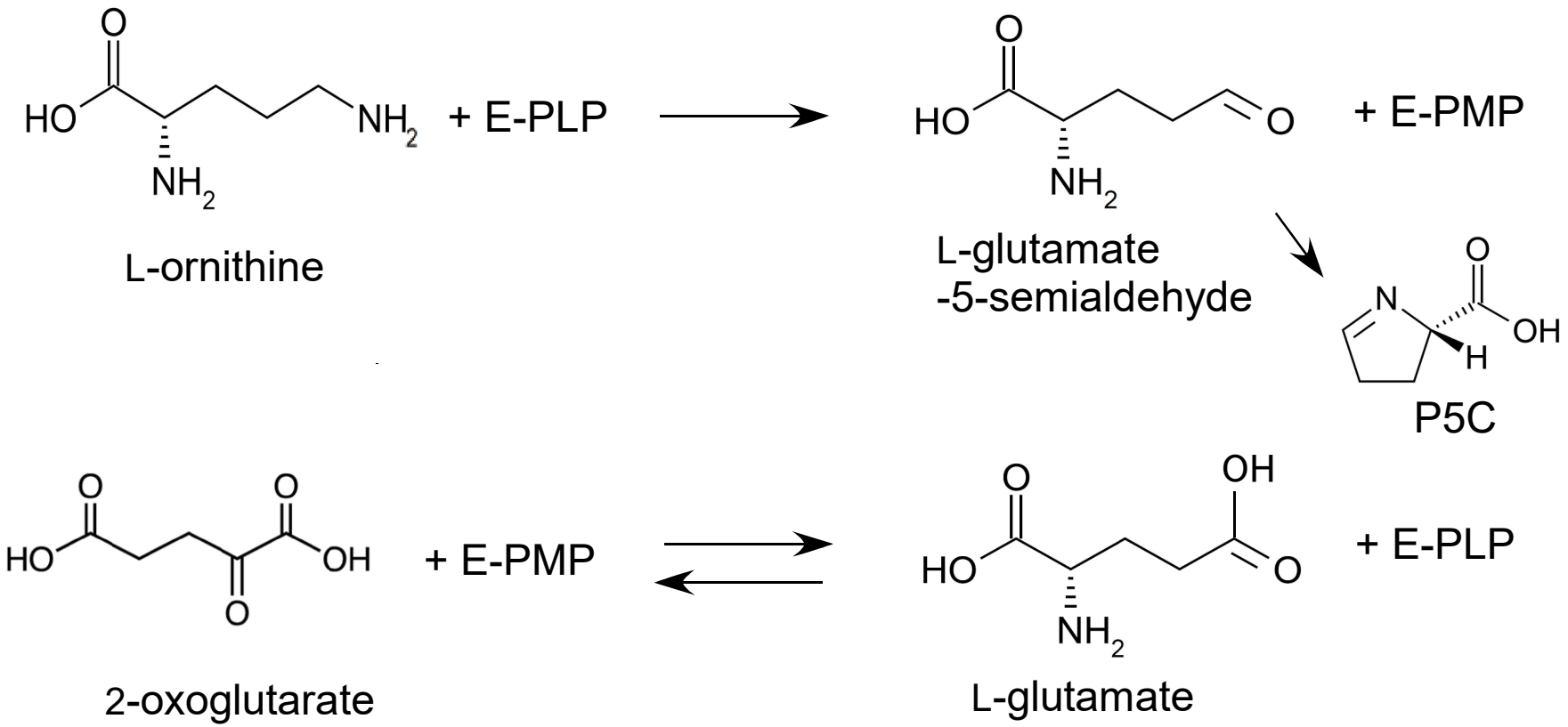
HO
O
NH2
NH2
+ E-PLP
L-ornithine
HO
O
NH2
O
+ E-PMP
L-glutamate
-5-semialdehyde
N
O
OH
H
P5C
HO
O
O
OH
O
+ E-PMP
2-oxoglutarate
HO
O
OH
NH2
O
+ E-PLP
L-glutamate

Fig. 1

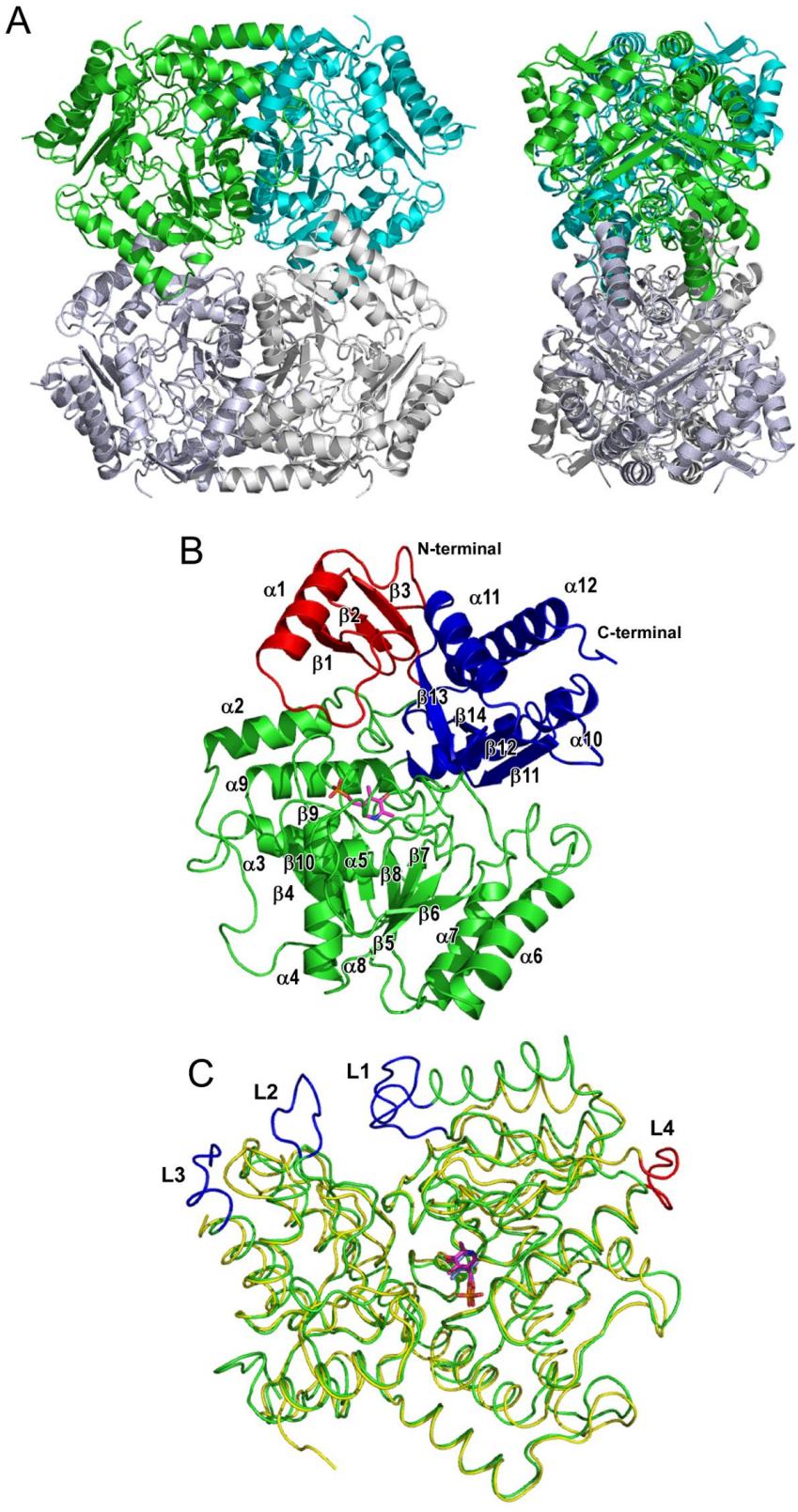
A
B
N-terminal
α1
β3
α11
α12
β2
C-terminal
β1
β13
α2
β14
α10
β12
β11
α9
β9
α3
β10
α5
β7
β8
β4
β6
α7
β5
α6
α8
α4
C
L1
L2
L4
L3

Fig. 2

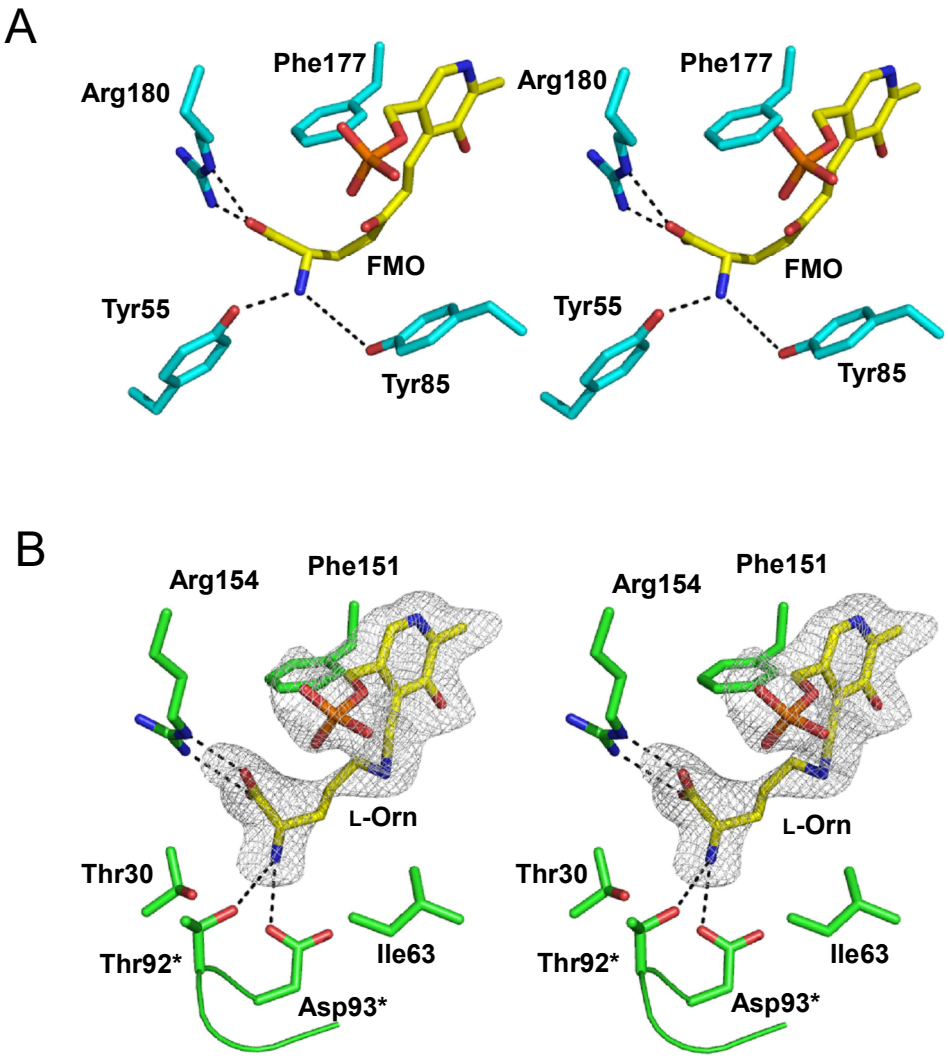
A
Arg180
Phe177
FMO
Tyr55
Tyr85
Arg180
Phe177
FMO
Tyr55
Tyr85
B
Arg154
Phe151
L-Orn
Thr30
Thr92*
Ile63
Asp93*
Arg154
Phe151
L-Orn
Thr30
Thr92*
Ile63
Asp93*

Fig. 3

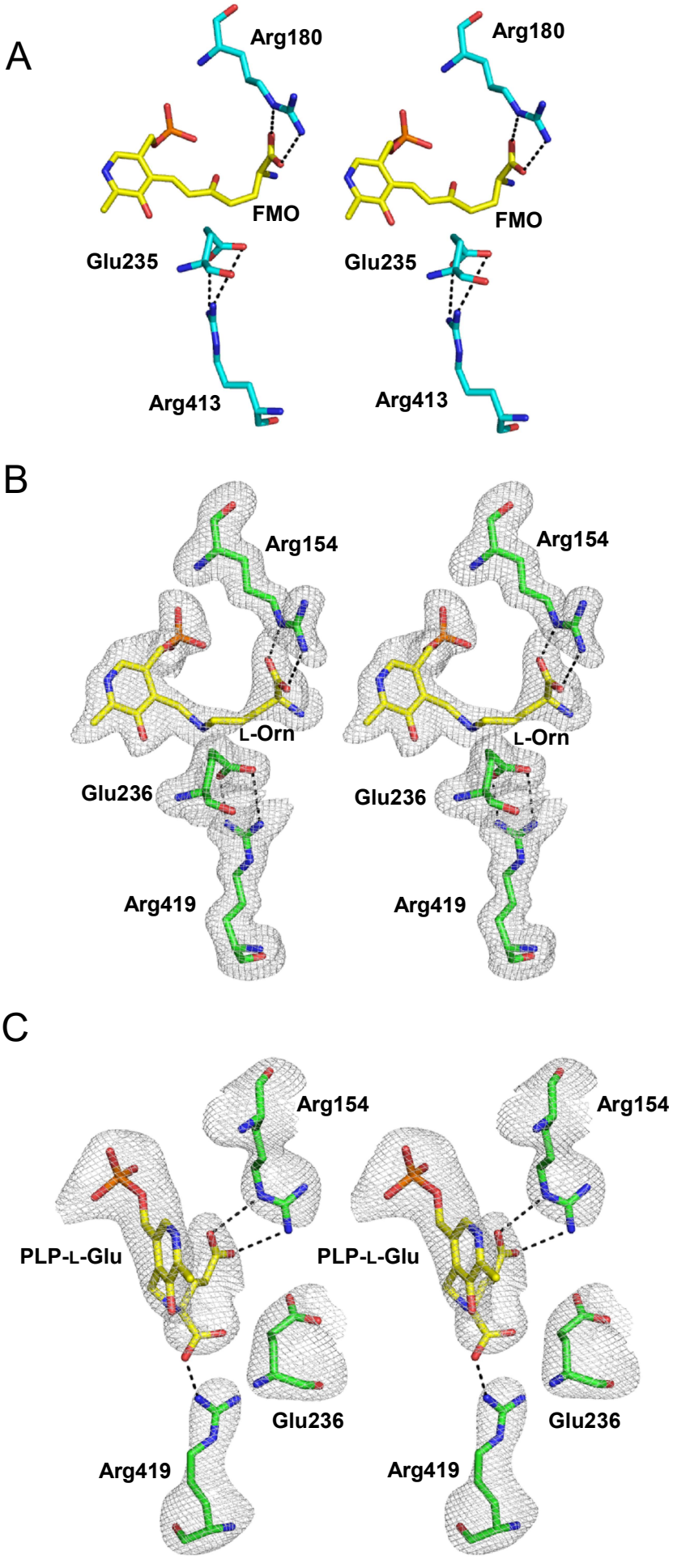
A
Arg180
FMO
Glu235
Arg413
Arg180
FMO
Glu235
Arg413
B
Arg154
L-Orn
Glu236
Arg419
Arg154
L-Orn
Glu236
Arg419
C
Arg154
PLP-L-Glu
Glu236
Arg419
Arg154
PLP-L-Glu
Glu236
Arg419

Fig. 4

Supplementary Table 1.

Primer sequences for site-directed mutagenesis.

T92V_Fw	GCTGGGGTAGACTACTATAACCCATAT
T92V_Rv	GTAGTCTACCCCAGCAGCGTGAAGTAC
D93L_Fw	GGGACTCTTTACTATAACCCATATCAA
D93L_Rv	ATAGTAAAGAGTCCCAGCAGCGTGAAG

Table 2 Kinetic analyses of Orn-AT

Amino donor	L-Orn	D-Orn	L-Lys	D-Lys
[2-Oxoglutarate]	10 mM	5 mM	10 mM	20 mM
k_{cat} (/sec)	4.32 ± 0.204	0.493 ± 0.0300	1.61 ± 0.0740	3.25 ± 0.250
K_m (mM)	0.106 ± 0.0136	0.446 ± 0.0804	0.211 ± 0.0216	5.22 ± 0.854
k_{cat}/K_m (/sec/mM)	40.8± 5.57	1.11± 0.210	7.60± 0.851	0.623± 0.113

Amino acceptor	2-Oxoglutarate			
[Amino donor]	1 mM L-Orn	5 mM D-Orn	2 mM L-Lys	20 mM D-Lys
k_{cat} (/sec)	3.51 ±0.170	0.462 ± 0.023	1.41 ± 0.050	3.02 ± 0.095
K_m (mM)	0.802 ± 0.122	0.182 ± 0.028	0.624 ± 0.077	1.23 ± 0.103
k_{cat}/K_m (/sec/mM)	4.38± 0.697	2.54± 0.417	2.26± 0.290	2.46± 0.220

Table 3. Data-collection and refinement statistics for *P. horikoshii* Orn-AT.

	PLP-bound enzyme	L-Orn/PLP-bound enzyme	PLP-L-Glu-bound enzyme
PDB code	7vno	7vnt	7vo1
Data collection			
Synchrotron light source	Photon Factory	Photon Factory	Photon Factory
Beamline	AR- NW12A	AR- NW12A	AR- NW12A
Wavelength (Å)	1.0	1.0	1.0
No. of frames	360	360	360
Oscillation width (deg)	0.5	0.5	0.5
Detector distance (mm)	201.1	201.1	364.7
Exposure per frame (s)	1	1	1
Temperature (K)	100	100	100
Indexing and scaling			
Space group	$P6_522$	$P6_522$	$P6_522$
Unit cell parameters			
a (Å)	113.4	113.8	113.7
b (Å)	113.4	113.8	113.7
c (Å)	290.0	289.6	290.7
α (°)	90	90	90
β (°)	90	90	90
γ (°)	120	120	120
Resolution range (Å) [a]	50–1.80 (1.83–1.80)	50–1.92 (1.95–1.92)	50–2.99 (3.04–2.99)
Total No. of reflections	1426382	1640791	438239
No. of unique reflections	102595	84821	23423
Redundancy [a]	13.9 (12.8)	19.3 (18.4)	18.7 (16.2)
Completeness (%)[a]	100 (100)	99.5 (99.0)	100 (99.9)
$< I/\sigma(I) >$ [a]	5.3 (2.3)	4.0 (2.1)	5.9 (2.2)
R_{merge} [a, b]	0.133 (0.713)	0.126 (1.16)	0.069 (0.924)
R_{pim} [a, c]	0.035 (0.19)	0.029 (0.28)	0.016 (0.23)
$CC_{1/2}$ [a, d]	0.998 (0.975)	1.000 (0.962)	1.000 (0.929)
No. of chains per asymmetric unit	2	2	2
Refinement			

Resolution range (Å)	50–1.80	50–1.92	50–2.99
R/R_{free} (%) [a, e]	17.3/20.2	18.1/21.5	22.0/28.4
	(24.0/26.4)	(22.7/23.8)	(30.7/37.8)
No. of protein atoms	7130	7130	7130
No. of water molecules	641	564	29
No. of ligands	Ethylene glycol, 3	Ethylene glycol, 1	
	Glycerol, 2	Glycerol, 1	
	PLP, 2	PLP, 2	
		L-Ornithine, 1	
			PLP-L-Glu, 2
Average B-factors (Å^2)	26.6	31.3	105
R.m.s.d.			
Bond lengths (Å)	0.012	0.011	0.011
Bond angles (°)	1.7	1.7	1.2
Ramachandran statistics			
Favored (%)	94.3	95.0	92.4
Allowed (%)	5.7	5.0	7.6
Outliers (%)	0	0	0

[a] Values in parentheses: highest resolution data shell; r.m.s.d.: root-mean-square deviation.

[b] $R_{merge} = \sum_{hkl} \sum_i | I_i(hkl) - \langle I(hkl) \rangle | / \sum_{hkl} \sum_i Ii(hkl)$, where $I_i(hkl)$ is the scaled intensity of the ith observation of reflection hkl. $\langle I(hkl) \rangle$ is the mean value and summation over all measurements.

[c] $R_{pim} = \Sigma_h [1/ (/n_h - 1)]^{1/2} \Sigma_i | < I_h > - I_{h,i}| / \Sigma_h \Sigma_i I_{h,I}$, where h enumerates the unique reflections, i represents their symmetry-equivalent contributors, and n_h denotes multiplicity.

[d] $CC_{1/2}$ = Correlation between intensities from random half-data sets.

[e] R_{free} calculated with randomly selected reflections (5%).